EurJIC
European Journal of Inorganic Chemistry

Research Article
doi.org/10.1002/ejic.202100923

Chemistry Europe
European Chemical Societies Publishing

www.eurjic.org

A P-Functionalized [3]Ferrocenophane with a Dynamic SPS-Bridge

Stefan Weller,[a] Robert Klenk,[a] Zsolt Kelemen,*[b] László Nyulászi,[b] Martin Nieger,[c] and Dietrich Gudat*[a]

Ferrocene-1,1′-dithiol reacts with PCl_3 and $P(NMe_2)_3$ to give [3]ferrocenophanes with SPS-*ansa*-bridges comprising potentially reactive P–Cl and P–N bonds at the central bridge atom. The products were characterized by NMR data and single-crystal XRD studies. The P-chloro-derivative exists both in the solid state and in solution as a mixture of two energetically nearly degenerate conformers with different stereochemical disposition of the *ansa*-bridge. Activation parameters for the dynamic equilibration between both isomers in solution were determined by dynamic NMR spectroscopy. Computational studies suggest that the isomerization proceeds via a torsional motion of the bridging SPS-unit rather than via configuration inversion at the phosphorus atom.

Introduction

Linking the cyclopentadienyl (Cp) units in a ferrocene derivative by one or more covalent bridges is a well-established approach to engineer not only the molecular structures of the original species but also their physical and chemical properties.[1] The impact of the bridge on the properties of the resulting ferrocenophane or *ansa*-ferrocene molecules can in principle arise from structural effects, the introduction of new chemical functionality, or a combination of both. Structure induced changes may be a simple consequence of the inhibition of the free rotation of the Cp units, which enables e.g. constructing chiral ferrocene scaffolds,[2] or can arise from enforcing geometrical distortions like a tilt between the Cp rings in strained ferrocenophanes, which allows tuning the optical properties of the ferrocene chromophore.[3] An easy approach to introducing new chemical functionality is doping the bridging unit with heteroatoms that enable complex formation with external substrates. Appropriate ferrocene-decorated P- or N-donor ligands are often based on [3]ferrocenophane scaffolds (**I**, Scheme 1)[4] whose bridge imposes little strain to grant chemically stable molecular structures, and have received attention as switchable ligands whose donor and acceptor properties are easily tunable by redox reactions at the iron center.[5]

We and others have recently reported on the synthesis of phosphorus-containing [3]ferrocenophanes **II** with *ansa*-bridges comprising a central tervalent phosphorus atom and two adjacent heteroatoms X acting as pier units to the ferrocene moiety.[6,7] These species can act as P-donor ligands in the formation of transition metal complexes[5,6e,8] or, if the phosphorus atom carries a displaceable halogen substituent, as precursors to carbene-analogue phosphenium ions **III**.[9] The [3]ferrocenophane framework in these compounds plays on one hand an important role in providing a rigid molecular backbone enabling, e.g., the synthesis of configurationally stable chiral ligands.[6e] On the other hand, the possible existence of several diastereomers with different bridge configurations and maybe varying complexation behavior for species like **II** (X=PR′)[7e,f] may also interfere with the application of these ferrocenophanes in coordination chemistry. However, the configuration isomerization documented for some phosphines **II** (X=P*t*Bu)[7f] as well as a for a radical **IV**[7g] emphasizes that full understanding of the properties of XPX-[3]ferrocenophanes requires knowledge on not only their static but also their dynamic stereochemistry.

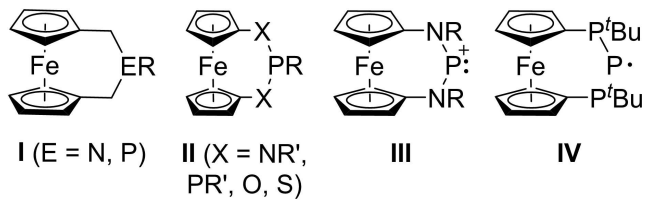

Scheme 1. Some known [3]ferrocenophane frameworks with *ansa*-bridges comprising a central group-15 element.

[a] Dr. S. Weller, R. Klenk, Prof. Dr. Dr. h. c. D. Gudat
Institut für Anorganische Chemie
University of Stuttgart
Pfaffenwaldring 55, 70550 Stuttgart, Germany
E-mail: gudat@iac.uni-stuttgart.de
https://www.iac.uni-stuttgart.de/forschung/akgudat/
[b] Dr. Z. Kelemen, Prof. Dr. L. Nyulászi
Department of Inorganic and Analytical Chemistry and MTA-BME Computation Driven Chemistry Research Group
Budapest University of Technology and Economics,
Szent Gellért tér 4, 1111 Budapest, Hungary
E-mail: kelemen.zsolt@vbk.bme.hu
[c] Dr. M. Nieger
Department of Chemistry
University of Helsinki,
P.O Box 55, 00014 University of Helsinki, Finland

Supporting information for this article is available on the WWW under https://doi.org/10.1002/ejic.202100923

Part of the "Ferrocene Chemistry" Special Collection.

Research Article
doi.org/10.1002/ejic.202100923

We report in this work on the synthesis and characterization of 1,3,2-dithiaphospha-[3]ferrocenophanes (**1**, **2** Scheme 2) that we consider special in two respects. Firstly, the synthesis of type-**II** [3]ferrocenophanes with P–Cl or P–N-bonds that allow in principle for further post-derivatization of the *ansa*-bridge has been reported for species with X=O,[6d] NR′,[7d,h] and PR′,[7f] but not for the thia-derivatives with X=S. Secondly, P-chloro-substituted **1** offers an unprecedented opportunity to monitor the bridge-dynamics in a ferrocenophane-based phosphine, which was not directly spectroscopically observable in **II** (X=P*t*Bu)[7f] and **IV**.[7g] Interpretation of the resulting kinetic data in combination with computational studies provides insight into the conformational mobility and isomerization mechanism of the *ansa*-bridge.

Results and Discussion

Although the inadvertent generation of **1** as a side product and its isolation in low yield (ca. 5%) has been mentioned in a conference report,[6b] characterization data are unavailable. We found that **1** is readily accessible through spontaneous condensation of ferrocene-1,1′-dithiol with phosphorus trichloride (Scheme 2) and can be obtained as a crude product in 97% yield by stripping of volatiles from the reaction mixture. The use of an auxiliary base as hydrogen chloride scavenger causes, in accord with a previous report,[6b] side reactions and impedes work-up, and is thus considered detrimental. In a similar manner, we were able to prepare 2-amino-substituted [3]ferrocenophane **2** from ferrocene-1,1′-dithiol and tris(dimethylamino)phosphine. Recrystallization of the crude products gave decent yields (**1**: 55%, **2**: 59%) of crystalline materials that were characterized by single-crystal X-ray diffraction studies.

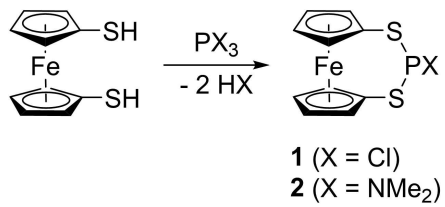

Scheme 2. Synthesis of 1,3,2-dithiaphospha-[3]ferrocenophanes **1**, **2**.

Both crystals studied contain isolated complexes lacking any significant intermolecular interactions. The asymmetric unit of **1** comprises two crystallographically independent molecules which exhibit both an ecliptic alignment of the Cp-decks in the ferrocene unit but are distinguished by different conformations of the *ansa*-bridge (Figure 1). For an analysis of the deviations between both conformers, it is convenient to consider the atoms of the SPS-unit, the adjacent carbon atoms (C5/C5′ and C9/C9′), and the iron center as constituents of a six-membered heterocycle. Seeing that the phosphorus atom is displaced from a common plane defined by the remaining ring constituents, we assign the ring a sort of envelope conformation and identify the SPS-unit as the flap of this envelope.[10] Adopting this view, one conformer is characterized by a flattened disposition of the envelope (with a flap angle between the SPS-bridge and the planar fragment of the heterocycle of 134°) and a flagpole orientation of the P–Cl bond (as this bond is aligned close to the ferrocene unit, we denote this conformer as *endo*-**1**), while the other one (*exo*-**1**) features a strongly folded envelope shape (flap angle 100°) and an equatorial orientation of the P–Cl bond. The opening of the envelope associated with the increase in flap angles comes with an expectable widening of the C–S–P angles from 95° in *exo*-**1**, which is a typical bond angle in sulfur compounds, to 110° in *endo*-**1** (see Table 1 for details). The concurrent change from equatorial (*exo*-**1**) to flagpole orientation (*endo*-**1**) of the P–Cl bond is associated with a flattening of the pyramidal coordination geometry around the phosphorus atom. Similar deviations between *exo*- and *endo*-conformers are also known for other XPX-[3]ferrocenes (X=N, O, P)[5c,d,6d,7] and reflect presumably the impact of repulsive interactions between the P-substituents in the *endo*-conformers and the adjacent ferrocene unit. The P–S and P–Cl distances in both isomers come close to those expected for normal single bonds (P–S 2.12 Å, P–Cl 2.09 Å[11]), but careful comparison reveals that the more open envelope shape in *endo*-**1** features slightly contracted P–Cl and elongated P–S distances, respectively (Table 1). The structural features of the ferrocene units are normal.

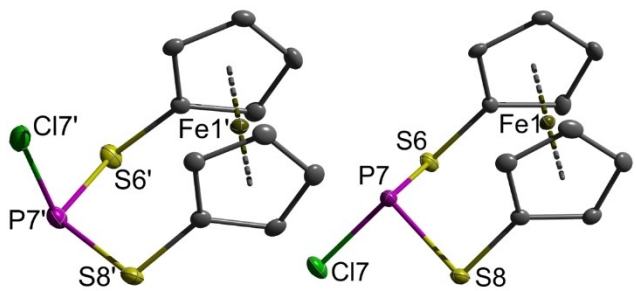

Figure 1. Representation of the molecular structures of a) *endo*-**1** (left) and b) *exo*-**1** (right) in the crystal. Hydrogen atoms were omitted for clarity and thermal ellipsoids were drawn at the 50% probability level. See Table 1 for selected distances and angles.

Table 1. Selected geometric parameters (distances in Å and angles in °) for **1** and **2**.

Parameter[a]	*exo*-**1**	*endo*-**1**	**2**[b]	
P7–X[c]	2.0739(11)	2.0902(11)	1.663(7)	1.658(7)
P7–S6	2.1308(11)	2.0942(11)	2.153(3)	2.156(3)
P7–S8	2.1234(10)	2.0915(12)	2.160(3)	2.159(3)
C5–S6–P7	95.13(10)	110.35(10)	98.8(3)	100.8(3)
C9–S8–P7	95.23(10)	110.82(10)	99.3(3)	100.0(3)
$\Sigma<$(P)[d]	296.54(12)	315.96(15)	299.5(7)	299.5(7)
$\Sigma<$(N)[d]			356.5(19)	359.8(19)
Cp···Cp[e]	3.3104(8)	3.2798(8)	3.3043(24)	3.2914(24)
α[f]	0.88(11)	1.54(13)	2.0(3)	2.1(3)

[a] Atom labels in *endo*-1 and the second molecule of **2** are S6′, P7′ etc. [b] values for two crystallographically independent molecules with *exo*-oriented P–N bond. [c] X=Cl7 (**1**), N70 (**2**). [d] Sum of bond angles. [e] Distance between the centroids of the Cp-rings. [f] Tilt angle between the Cp-decks (see ref. [1e]).

Research Article
doi.org/10.1002/ejic.202100923

Crystals of **2** hold likewise two crystallographically independent molecules (Figure 2), both of which can be assigned as *exo*-conformers with flap angles of 107° and 110°, respectively. The preference for this conformation is well in accord with the greater steric demand of the Me_2N-substituent compared to the Cl-atom in **1**. As in **1**, the structural features of the ecliptic ferrocene unit are normal and require no comment. The bond angles at the phosphorus and sulfur atoms adopt values between those in both conformers of **1**, but are definitely closer to those of *exo*-**1** displaying the same conformation of the *ansa*-bridge. The P–S distances are slightly larger than in *exo*-**1**, but still in accord with the presence of single bonds. In combination with the essentially planar geometry around the nitrogen atom (which implies a high degree of p-character for the N-centered lone-pair) and a rather short P–N distance (1.66 Å compared to 1.78 Å for a standard single bond[11]), this trend may be attributed to n(N)–σ*(PS) hyperconjugation. Indeed, a second order perturbation theory analysis of the calculated (at the ωB97X-D/6-311 + G** level of theory) electron density on the NBO basis reveals 96.2 kJ mol^{-1} stabilizing interactions between the lone pair of the nitrogen and the σ*(PS) orbitals, which are also reflected in the shapes of the HOMO and LUMO (Figure S8). Analogous interactions are well established for other types of amino-substituted heterocyclic phosphines.[12]

The different conformational preferences of **1** and **2** unveiled in the crystallographic studies also show up in the solution NMR data. In the case of **2**, the $^{31}P\{^1H\}$ and ^1H NMR spectra display a singlet and a set of resonances attributable to the AHMX spin system of the H-atoms in the equivalent Cp-decks, respectively. These patterns are well in accord with the presence of a single conformer in solution, which has presumably the same *exo*-orientation of the amino-substituent as observed in the crystalline state. In contrast, the $^{31}P\{^1H\}$ NMR spectrum of **1** displays at ambient temperature an extremely broad signal ($\delta^{31}P = 180$ ppm, $\Delta\nu_{1/2}$ approx. 4 kHz), which decoalesces eventually into two singlets with distinctly differing chemical shifts ($\delta^{31}P = 218.8$ and 139.5 ppm at 199 K) when the temperature is lowered (Figure 3).

Parallel variations are also evident in the ^1H NMR spectrum, where the signals of a single set of Cp-resonances detectable at room temperature likewise split into two AHMX-type patterns at lower temperatures (Figure S5). The observed changes clearly indicate that the solution contains a mixture of dynamically equilibrating species, which we allot to the conformers *exo*-**1** and *endo*-**1** identified in the solid state. A similar variation in ^{31}P chemical shifts as noted here ($\Delta\delta^{31}P = 79.3$ ppm) was reported for diastereomeric triphospha-[3]ferrocenophanes[7f] and some bicyclic phosphines[13] ($\Delta\delta^{31}P = 50$–90 ppm). Our tentative assignment is confirmed by the close agreement of the observed chemical shifts with calculated values (at the zora-BP86/TZ2P//ωB97X-D/6-311 + G** level of theory),[14] which allow also to attribute the signal at higher chemical shift to the *endo*-isomer (*endo*-**1**: $\delta^{31}P_{calc} = 219.1$ vs. $\delta^{31}P_{obs} = 218.8$ at 199 K, *exo*-**1**: $\delta^{31}P_{calc} = 143.1$ vs. $\delta^{31}P_{obs} = 139.5$ at 199 K).

Computational studies on bicyclic phosphines[13] revealed that the large deviations between the ^{31}P chemical shifts of different stereoisomers stem from changes of the paramagnetic magnetic shielding contribution induced by structure-dependent fine-tuning of hyperconjugative interactions of the phosphorus lone-pair and the bond to the exocyclic substituent with unoccupied fragment orbitals in the bicyclic framework. Indeed, the difference in $\delta^{31}P$ between *endo*/*exo*-**1** is also clearly dominated by changes in the paramagnetic shielding term, with only a small contribution from the spin-orbit term (Table S7), and inspection of canonical Kohn-Sham orbitals (see Figure S8) and the results of NBO calculations reveals that the hyperconjugative interactions at phosphorus and its neighbors differ in both isomers as expected. Moreover, the NBO calculations show that the phosphorus lone pair of *exo*-**1**

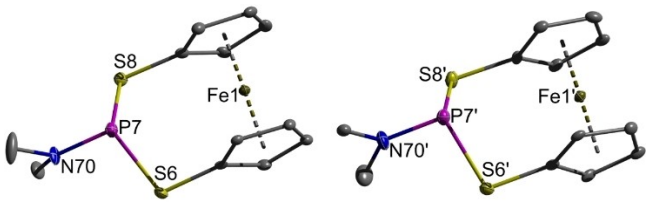

Figure 2. Representation of the molecular structures of the crystallographically independent molecules of **2** in the crystal. Hydrogen atoms were omitted for clarity and thermal ellipsoids were drawn at the 50% probability level. See Table 1 for selected distances and angles.

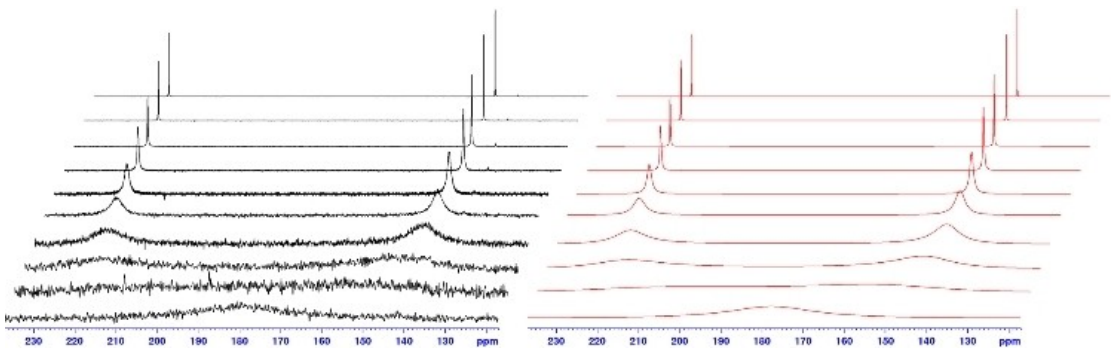

Figure 3. Measured (black traces) and simulated (red traces) $^{31}P\{^1H\}$ NMR spectra of **1** at different temperatures (from top to bottom: 199, 211, 223, 234, 246, 257, 269, 281, 292, 304 K).

Research Article
doi.org/10.1002/ejic.202100923

displays increased *s*-character and makes a smaller contribution to the paramagnetic shielding term, implying that part of the difference in δ^{31}P between *exo*/*endo*-**1** is caused by rehybridization effects. However, even if these findings imply that the stereochemically induced variation of δ^{31}P for *endo*/*exo*-**1** has a similar origin as in the previously studied phosphines,[13] attempts to relate the observed trend with individual orbital contributions gave no clear picture, and a more detailed discussion is currently out of reach.

Insight into the energetics and kinetics of the conformational isomerization *endo*-**1**⇆*exo*-**1** was available from a more detailed analysis of the variable temperature NMR experiments on **1**. Integration of the signals in ^{31}P NMR spectra recorded in the slow exchange regime furnished values of the equilibrium constant $K^{endo/exo}$(T), and evaluation of the temperature dependence of this quantity from a van-t'Hoff plot (see Figure S6) allowed then to determine the change in enthalpy ($\Delta H = -0.53(3)$ kJ/mol) and entropy ($\Delta S = -0.63(12)$ J/(mol K) associated with the reaction. The figures obtained imply that *exo*-**1** must be regarded energetically marginally more stable, but this preference is very small and in part compensated by the entropy term.

Rate constants for the dynamic isomerization were extracted from line shape analyses of the ^{31}P and ^{1}H NMR signals and employed to calculate the enthalpy and entropy of activation by means of the Eyring equation (see Figure S7). The enthalpic barrier to the *endo*-**1**⇆*exo*-**1** isomerization ($\Delta H^{\neq} =$ 41.9(9) kJ/mol) matches those for the degenerate bridge reversal in 1,3-dithia-[3]ferrocenophanes **3** (Scheme 3, $\Delta H^{\neq} =$ 40–45 kJ/mol),[15] but is only roughly half as high as the isomerization barrier of trithia-[3]ferrocenophane **4a** ($\Delta H^{\neq} =$ 77.0(9) kJ/mol)[16] featuring an *ansa*-bridge with a similar metrical chain length as **1** (minor differences are due to the shortening of the S–S distances of 2.048(4) and 2.050(4) Å[17] compared to the P–S bonds in **1**). Although the lower transition state energy for **1** is to some extent offset by a more negative activation entropy ($\Delta S^{\neq} = -19.8$ (3.7) J/(mol·K) vs. −11.7(2.3) J/(mol·K) for **4a**[16]), which implies a higher degree of order in the transition state of the isomerization, the values of $\Delta G^{298,\neq}$ (47.8(5) kJ/mol for **1** vs. 80.4(2) kJ/mol for **4**[16]) suggest that the conformational flexibility of the *ansa*-bridge increases upon formal replacement of the central sulfur atom in **4a** by a PCl unit.

Even if one considers that the ring flip in tri-chalcogen-bridged [3]ferrocenophanes becomes energetically more facile when the central sulfur in **4a** is formally replaced by increasingly larger selenium or tellurium centers,[16] the gain in mobility of **1** is too high to be attributable to geometrical effects alone. Moreover, the case of **1** is more complex (cf. Figure 4). The interchange between the *endo*- and *exo*-isomer can occur here as in **4a** via a torsional motion of the ring involving a transition state TS_{flip}-**1** in which the ferrocene unit shows a staggered orientation of the Cp-decks and a twisted conformation of the *ansa*-bridge while the phosphorus atom retains a fixed pyramidal coordination. Alternatively, the same isomerization can be accomplished through configuration inversion at the phosphorus center (TS_{inv}-**1**).

Seeking to assess the viability of both routes, we have studied the conversion *endo*-**1**⇆*exo*-**1** computationally. The ωB97X-D/6-311 + G** model, which had already been identified in a previous case as suitable for the depiction of ferrocenophane systems,[9] was found to give also a realistic account of the molecular structures of *endo*/*exo*-**1** and **2**, and was used for energy optimization of geometries. The energies of molecular ground states and transition states thus located were then recomputed at the local-CCSD(T)/def2-TZVP//ωB97X-D/6-311 + G** level and Gibbs free energies (at 298 °K) calculated using these energies with corrections derived from frequency calculations at the ωB97X-D/6-311 + G** level of theory. The Gibbs energy difference between both conformers of **1** at this theoretical level (which will be used throughout the following discussion) was computed as 6.4 kJ/mol (Figure 4), with *endo*-**1** being identified as the more stable isomer (the same energetic order was reproduced at other theoretical levels, even if the absolute energy difference varied between 2.1 and 11.3 kJ/mol; see Table S4 for details). Although a higher stability of *endo*-**1** is at odds with our experimental results, the deviations between calculated and measured Gibbs free energy differences are well within the 8–12 kJ/mol error limit that must be conceded for

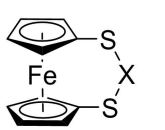

X = CH_2 (**3a**), CMe_2 (**3b**)
X = S (**4a**), Se (**4b**), Te (**4c**)

Scheme 3. Molecular structures of some 1,3-dithia-[3]ferrocenophanes **3**, **4**.

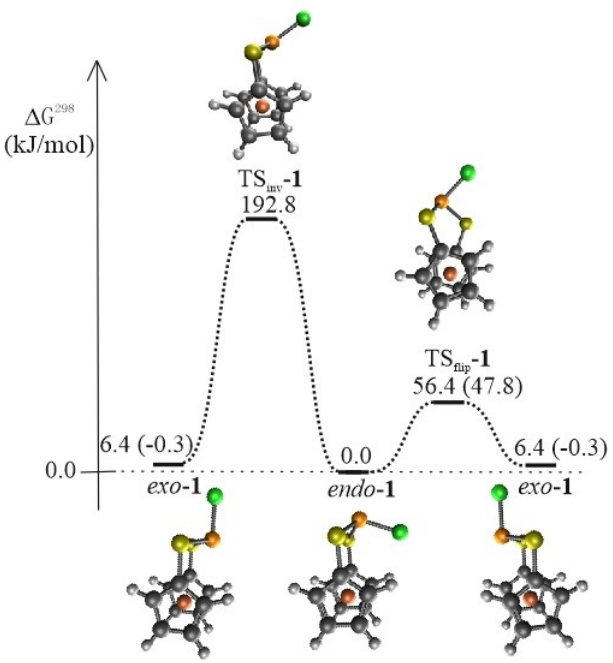

Figure 4. Representation of studied pathways for the dynamic isomerization *endo*-**1**⇆*exo*-**1**. The numbers shown represent the calculated and experimental (in parentheses) relative Gibbs free energies in kJ/mol.

DFT calculations. Therefore, we attribute our failure in predicting a correct energetic order to the methodical limits rather than inappropriateness of our model.

Analyzing next the reaction dynamics, we have located two transition states that can be associated with the suggested routes involving either direct inversion at the phosphorus atom or a torsional ring flip, respectively (Figure 4). The transition state TS_{inv}-**1** localized for the inversion process has a similar trigonal planar geometry ('umbrella' or 'vertex'-type) as is encountered in case of triorgano- or trithiophosphines.[18] The energetic barrier for P-inversion in **1** derived from the DFT calculations ($\Delta G^{298\neq} = 192.8$ kJ/mol relative to *endo*-**1**) is intermediate between the inversion barriers for trithiolato-phosphines $P(SR)_3$ (R=H, Me)[18] and PCl_3,[18,19] respectively. The P-inversion is clearly disfavored with respect to the torsional ring flip (via TS_{flip}-**1**) with a predicted energetic barrier ($\Delta G^{298\neq} =$ 56.4 kJ/mol) that fits reasonably well with the experimental value ($\Delta G^{298\neq} = 47.8$ kJ/mol). We further found a somewhat higher energy path, which permits epimerization of *exo*-**1** via joint inversion of both the envelope conformation of the ferrocenophane ring and the pyramidal coordination at phosphorus via a transition state (Figure S9, $\Delta G^{298\neq} = 193.8$ kJ/mol) with planar FeC_2S_2P-ring and similar T-shaped geometry at phosphorus as in the 'edge-type TS' passed during inversion of PCl_3.[18,19] However, the absence of any evidence for dynamic symmetrization of the Cp-rings in the ^{1}H NMR spectra indicate that this process is unrelated with the observed dynamics.

To validate our computational model, we calculated also the inversion barrier for the ring flip of **4a** and note that the still closer agreement between the computed ($\Delta G^{298\neq} = 84.6$ kJ/mol) and measured ($\Delta G^{298\neq} = 80.4$ kJ/mol[16]) data indicates the predicted energy barriers can be considered reasonable. Based on this data, we presume that, as in the case of **4a**, interconversion between different conformers of **1** is achieved by torsional motion around the P–S bonds in the *ansa*-bridge.

An analogous survey of **2** (Table S5) revealed that a hypothetical *endo*-isomer is less stable by 19.0 kJ/mol than the observed *exo*-conformer. The reduced stability of *endo*-**2** is in accordance with the lack of n_N–σ^*_{PS} hyperconjugation that is evidenced by the non-planar nitrogen and the significantly lengthened (1.74 Å) P–N bond. Moreover, both the torsional ring flip ($\Delta G^{298\neq} = 43.3$ kJ/mol) and the inversion process ($\Delta G^{298\neq} = 164.2$ kJ/mol) become more facile than in case of **1**. These figures indicate that the failure to detect a second conformer of **2** is not owed to kinetic effects, but reflects rather the very low equilibrium concentration of this isomer.

Conclusion

1,3,2-Dithiaphospha-[3]ferrocenophanes with potentially reactive P–X bonds (X=Cl, NMe_2) offering an opportunity for further post-functionalization can be prepared by analogy to their O_2P-bridged congeners via condensation of ferrocene-1,1′-dithiol with PX_3 in the absence of base. The P-chloro derivative is characterized by an accidental energetic near-degeneracy of two conformers that are set apart by an *exo*- or *endo*-orientation of the P–Cl bond in the *ansa*-bridge relative to the ferrocene core. Monitoring the dynamic interchange between both species by VT-NMR spectroscopy enabled for the first time evaluating activation parameters for the bridge reversal in a phosphorus-containing [3]ferrocenophane, which imply that the SPS-chain is more flexible than the SES-units (E=S, Se, Te) in trichalcogeno-[3]ferrocenophanes. Computational studies suggest that the conformational isomerization proceeds via a torsional motion of the SPS-bridge, which is energetically less costly than configuration inversion at the phosphorus atom.

Experimental Section

Unless otherwise stated, all manipulations were carried out under an inert atmosphere of purified argon, using either flame-dried glassware and standard Schlenk techniques, or in gloveboxes. THF was distilled from NaK alloy and stored in Schlenk-flasks under inert conditions. NMR spectra were acquired on Bruker Avance 250 (^{1}H: 250.0 MHz, ^{31}P: 101.2 MHz) or Bruker Avance 400 (^{1}H: 400.1 MHz, ^{31}P: 161.9 MHz) NMR spectrometers at 303 K if not stated otherwise. ^{1}H Chemical shifts were referenced to TMS using the signals of the residual protons of the deuterated solvent ($\delta^1H = 7.26$ ($CDCl_3$) as secondary reference. ^{31}P chemical shifts were referenced using the Ξ-scale[20] with 85 % H_3PO_4 ($\Xi = 40.480747$ MHz) as secondary reference. Elemental analyses were performed with an Elementar Micro Cube elemental analyser.

2-Chloro-1,3,2-dithiaphospha-[3]ferrocenophane (**1**). A solution of ferrocene-1,1′-dithiol (721 mg, 2.88 mmol) in THF (10 mL) was added dropwise over a period of 30 min to a cooled (−78 °C) solution of PCl_3 (396 mg, 252 μL, 2.88 mmol) in THF (10 mL). The cooling was removed and the reaction mixture stirred for 14 h. Evaporation of all volatiles in vacuum furnished 877 mg (2.79 mmol, 97 %) of crude product which was purified by recrystallization from THF and drying under vacuum. Yield 500 mg (1.59 mmol, 55 %) of a fine crystalline, orange solid of m.p. 120 °C. – ^{1}H NMR ($CDCl_3$): δ = 4.38 (m, 2 H, Cp), 4.33 (m, 2 H, Cp), 4.19 (m, 2 H, Cp), 4.07 (m, 2 H, Cp). – ^{31}P{^{1}H} NMR ($CDCl_3$): δ = 180 (very broad). – $C_{10}H_8ClFePS_2$ (314.57 g/mol): calcd. C 38.18 H 2.56, found C 38.69 H 2.68.

2-Dimethylamino-1,3,2-dithiaphospha-[3]ferrocenophane (**2**). A solution of ferrocene-1,1′-dithiol (487 mg, 1.95 mmol) in THF (15 mL) was added dropwise over a period of 30 min to a cooled (−78 °C) solution of $P(NMe_2)_3$ (320 mg, 360 μL, 1.96 mmol) in THF (5 mL). The cooling was removed and the reaction mixture stirred for 16 h. The resulting mixture was filtered through a bed of silica and precipitated solids washed with three portions of THF (20 mL). The combined filtrates were evaporated to dryness and the remaining dark brown solid recrystallized from THF. Yield 372 mg (1.15 mmol, 59 %) of a crystalline, brown solid of m.p. 142 °C. – ^{1}H NMR ($CDCl_3$): δ = 4.25 (m, 2 H, Cp), 4.23 (m, 2 H, Cp), 4.07 (m, 2 H, Cp), 3.87 (m, 2 H, Cp), 2.92 (d, $^3J_{PH} = 9.7$ Hz, 6 H, NCH_3). – ^{31}P{^{1}H} NMR ($CDCl_3$): 181 (s). – $C_{12}H_{14}FeNPS_2$ (323.19 g/mol): calcd. C 44.59 H 4.37 N 4.33, found C 44.18 H 4.54 N 4.57.

Crystallographic studies. X-ray diffraction data for **1** and **2** were collected at 100(2) K on a Bruker diffractometer equipped with a Kappa Apex II Duo CCD-detector and a KRYO-FLEX cooling device using Mo-K_α radiation ($\lambda = 0.71073$ Å). The structures were solved with direct methods (SHELXS-2014[21]) and refined with a full-matrix least squares scheme on F^2 (SHELXL-2014[21]). Semi-empirical absorption corrections from equivalents were applied. Non-hydrogen atoms were refined anisotropically and hydrogen atoms using a riding model. The crystal structure of **2** was refined as a 2-

component twin, BASF = 0.1528(30). The option TwinRotMat of the PLATON package[22] was used to create a HKLF 5 file, which was then used for the further refinement, which is therefore based exclusively on unique reflections ($R_{int} = 0.00$). Due to the weakly scattering crystal, a cutoff at $\theta = 25°$ was employed, and refinement was carried out with a general RIGU restraint. Further crystallographic data and refinement details are given in the supporting information or in the cif-files.

Computational details. The Gaussian 09 program package[23] was used for all computations but the calculation of Local-CCSD(T) energies and and relativistic magnetic shieldings. Energy optimization of the geometry of *endo*/*exo*-**1** were initially performed at different levels of theory (see Table S4). Based on a comparison of the results with the experimental data, the ωB97X-D/6-311 + G** model, which had already been used in a previous case,[9] was chosen for all geometry optimizations and ensuing harmonic vibrational frequency calculations employed to check the nature of the stationary points obtained. Non-relativistic magnetic shieldings were computed at the BP86/cc-pVTZ//ωB97X-D/6-311 + G** level of theory. Calculations of magnetic shieldings employing the two-component zero-order regular approximation (ZORA) for inclusion of spin-orbit coupling[24] were carried out with the Amsterdam Density Functional package (ADF 2019.3)[25] using an all-electron, triple-ζ, double-polarization (TZ2P) Slater basis with the local density approximation (LDA) in the Vosko-Wilk-Nusair parameterization[26] and nonlocal corrections for exchange (Becke88[27]) and correlation (Perdew86[28]). Calculated magnetic shieldings were converted into ^{31}P NMR chemical shifts using the equation $\delta^{31}P(\text{analyte}) = (\sigma(PCl_3) - \sigma(\text{analyte}) + 219.0)$. Local-CCSD(T) calculations were carried out with the MRCC program package.[29] Molden 4.0[30] and IQmol 2.15.0[31] were used for the visualization of the computed structures and orbitals.

Deposition Numbers 2078920 (for **1**) and 2078927 (for **2**) contain the supplementary crystallographic data for this paper. These data are provided free of charge by the joint Cambridge Crystallographic Data Centre and Fachinformationszentrum Karlsruhe Access Structures service www.ccdc.cam.ac.uk/structures.

Acknowledgements

Financial support by the German Research Foundation (DFG) through grant no. GU 415/16-1 is gratefully acknowledged. We further thank B. Förtsch for elemental analyses, and Dr. W. Frey (Institute of Organic Chemistry, University of Stuttgart) for the collection of X-ray data sets. Z. K. is grateful for the general support of the Premium Postdoctoral Research Program 2019. We thank an unknown reviewer for his helpful comments on the discussion of the configuration inversion at phosphorus. Open Access funding enabled and organized by Projekt DEAL.

Conflict of Interest

The authors declare no conflict of interest.

Data Availability Statement

The data that support the findings of this study are available in the supplementary material of this article.

Keywords: Conformation analysis · Ferrocenes · Phosphanes · Phosphorus heterocycles · Sulfur heterocycles

[1] Selected reviews: a) W. E. Watts, *Organomet. Chem. Rev.* **1967**, *2*, 231–254; b) J.-S. Park, T. R. Lee in *Modern Cyclophane Chemistry* (Eds. R. Gleiter, H. Hopf), Wiley-VCH, Weinheim, **2004**, pp. 131–157; c) K. Osakada, T. Sakano, M. Horie, Y. Suzaki, *Coord. Chem. Rev.* **2006**, *250*, 1012–1022; d) I. R. Butler, *Eur. J. Inorg. Chem.* **2012**, 4387–4406; e) R. A. Musgrave, A. D. Russell, I. Manners, *Organometallics* **2013**, *32*, 5654–5667.
[2] K. Schlögl, *Pure Appl. Chem.* **1970**, *23*, 413–432.
[3] J. C. Green, *Chem. Soc. Rev.* **1998**, *27*, 263–272.
[4] a) T. Höcher, A. Cinquantini, P. Zanello, E. Hey-Hawkins, *Polyhedron* **2005**, *24*, 1340–1346; b) N. Fleury-Bregeot, A. Panossian, A. Chiaroni, A. Marinetti, *Eur. J. Inorg. Chem.* **2007**, 3853–3862; c) A. Voituriez, A. Panossian, N. Fleury-Bregeot, P. Retailleau, A. Marinetti, *J. Am. Chem.* **2008**, *130*, 14030–14031; d) N. Pinto, M. Neel, A. Panossian, P. Retailleau, G. Frison, A. Voituriez, A. Marinetti, *Chem. Eur. J.* **2010**, *16*, 1033–1045.
[5] a) L. Chen, X. Cui, H. Cheng, X. Chen, M. Song, M. Tang, D. Wei, X. Wu, *Appl. Organomet. Chem.* **2012**, *26*, 449–454; b) Q. Zhang, X. Cui, L. Zhang, S. Luo, H. Wang, Y. Wu, *Angew. Chem. Int. Ed.* **2015**, *54*, 5210–5213; *Angew. Chem.* **2015**, *127*, 5299–5302; c) E. Deck, H. E. Wagner, J. Paradies, F. Breher, *Chem. Commun.* **2019**, *55*, 5323–5326; d) B. S. Birenheide, F. Krämer, L. Bayer, P. Mehlmann, F. Dielmann, F. Breher, *Chem. Eur. J.* **2021**, *27*, 15067-15074..
[6] With X=O, S: a) A. G. Osborne, R. E. Hollands, R. F. Bryan, S. Lockhart, *J. Organomet. Chem.* **1985**, *288*, 207–217; b) M. Herberhold, C. Dörnhöfer, A. Scholz, G. X. Jin, *Phosphorus Sulfur Silicon Relat. Elem.* **1992**, *64*, 161–168; c) M. Herberhold, H.-D. Brendel, *J. Organomet. Chem.* **1993**, *458*, 205–209; d) M. Herberhold, A. Hofmann, W. Milius, *J. Organomet. Chem.* **1998**, *555*, 187–200; e) M. Neel, P. Retailleau, A. Voituriez, A. Marinetti, *Organometallics* **2018**, *37*, 797–801.
[7] With X=NR, PR: a) A. G. Osborne, H. M. Pain, M. B. Hursthouse, M. A. Mazid, *J. Organomet. Chem.* **1993**, *453*, 117–120; b) B. Wrackmeyer, E. V. Klimkina, W. Milius, *Inorg. Chem. Commun.* **2004**, *7*, 884–888; c) B. Wrackmeyer, E. V. Klimkina, W. Milius, *Z. Naturforsch.* **2009**, *64B*, 1401–1412; d) B. Wrackmeyer, E. V. Klimkina, W. Milius, *Z. Anorg. Allg. Chem.* **2010**, *636*, 784–794; e) C. Moser, F. Belaj, R. Pietschnig, *Phosphorus Sulfur Silicon Relat. Elem.* **2015**, *190*, 837–844; f) S. Borucki, Z. Kelemen, M. Maurer, C. Bruhn, L. Nyulászi, R. Pietschnig, *Chem. Eur. J.* **2017**, *23*, 10438–10450; g) S. Isenberg, S. Weller, D. Kargin, S. Valic, B. Schwederski, Z. Kelemen, C. Bruhn, K. Krekic, M. Maurer, C. M. Feil, M. Nieger, D. Gudat, L. Nyulászi, R. Pietschnig, *ChemistryOpen* **2019**, *8*, 1235–1243; h) S. Weller, S. H. Schlindwein, C. M. Feil, Z. Kelemen, D. Buzsáki, L. Nyulászi, S. Isenberg, R. Pietschnig, M. Nieger, D. Gudat, *Dalton Trans.* **2019**, *48*, 6236–6247.
[8] L.-M. Frenzel, C. Bruhn, R. Pietschnig, *Inorg. Chim. Acta* **2021**, *516*, 120091.
[9] S. Weller, S. H. Schlindwein, C. M. Feil, Z. Kelemen, D. Buzsáki, L. Nyulászi, S. Isenberg, R. Pietschnig, M. Nieger, D. Gudat, *Organometallics* **2019**, *38*, 4717–4725.
[10] The envelope conformation is commonly applied to characterize a particular conformation of five-membered rings featuring a single ring atom displaced from a common plane defined by the remaining atoms. The 'flap angle' denoted to describe the orientation of the flap of the envelope is defined as the angle X(C5,C9)–X(S6,S8)–P where X(A,B) denotes the center of the vector through atoms A, B.
[11] B. Cordero, V. Gómez, A. E. Platero-Prats, M. Revés, J. Echeverría, E. Cremades, F. Barragán, S. Alvarez, *Dalton Trans.* **2008**, 2832–2838.
[12] a) S. Burck, D. Gudat, F. Lissner, K. Nättinen, M. Nieger, T. Schleid, *Z. Anorg. Allg. Chem.* **2005**, *631*, 2738–2745; b) Z. Benkö, S. Burck, D. Gudat, M. Nieger, L. Nyulászi, N. Shore, *Dalton Trans.* **2008**, 4937–4945.
[13] D. B. Chesnut, L. D. Quin, K. D. Moore, *J. Am. Chem. Soc.* **1993**, *115*, 11984–11990.
[14] ^{31}P NMR chemical shifts computed at the non-relativistic BP86/cc-pVTZ//B3LYP/6-311 + G** (220.3 ppm for *endo*-**1** and 136.9 ppm for *exo*-**1**) and B3LYP/cc-pVTZ//B3LYP/6-311 + G** levels (210.4 ppm for *endo*-**1** and 143.8 ppm for *exo*-**1**) give the same assignment.
[15] E. W. Abel, M. Booth, C. A. Brown, K. G. Orrell, R. L. Woodford, *J. Organomet. Chem.* **1981**, *214*, 93–105.
[16] E. W. Abel, M. Booth, K. G. Orrell, *J. Organomet. Chem.* **1981**, *208*, 213–224.
[17] B. R. Davis, I. Bernal, *J. Cryst. Mol. Struct.* **1972**, *2*, 107–114.

[18] A. Espinosa Ferao, A. Garcia Alcaraz, *New J. Chem.* **2020**, *44*, 8763–8770.
[19] a) D. S. Marynick, *J. Chem. Phys.* **1980**, *73*, 3939–3943; b) D. A. Dixon, A. J. Arduengo, T. Fukunaga, *J. Am. Chem. Soc.* **1986**, *108*, 2461–2462; c) D. Buzsáki, Z. Kelemen, L. Nyulászi, *J. Phys. Chem. A.* **2020**, *124* (13), 2660–2671.
[20] R. H. Harris, E. D. Becher, S. M. Cabral de Menezes, R. Goodfellow, P. Granger, *Concepts Magn. Reson.* **2002**, *14*, 326–346.
[21] a) G. M. Sheldrick, *Acta Crystallogr.* **2015**, *C71*, 3–8; b) G. M. Sheldrick, *Acta Crystallogr.* **2008**, *A64*, 112–122.
[22] a) A. L. Spek, *Acta Crystallogr.* **2009**, *D65*, 148–155; b) A. L. Spek, *Acta Crystallogr.* **2015**, *C71*, 9–18.
[23] Gaussian 09, Revision E.01, M. J. Frisch, G. W. Trucks, H. B. Schlegel, G. E. Scuseria, M. A. Robb, J. R. Cheeseman, G. Scalmani, V. Barone, B. Mennucci, G. A. Petersson, H. Nakatsuji, M. Caricato, X. Li, H. P. Hratchian, A. F. Izmaylov, J. Bloino, G. Zheng, J. L. Sonnenberg, M. Hada, M. Ehara, K. Toyota, R. Fukuda, J. Hasegawa, M. Ishida, T. Nakajima, Y. Honda, O. Kitao, H. Nakai, T. Vreven, J. A. Montgomery, Jr., J. E. Peralta, F. Ogliaro, M. Bearpark, J. J. Heyd, E. Brothers, K. N. Kudin, V. N. Staroverov, T. Keith, R. Kobayashi, J. Normand, K. Raghavachari, A. Rendell, J. C. Burant, S. S. Iyengar, J. Tomasi, M. Cossi, N. Rega, J. M. Millam, M. Klene, J. E. Knox, J. B. Cross, V. Bakken, C. Adamo, J. Jaramillo, R. Gomperts, R. E. Stratmann, O. Yazyev, A. J. Austin, R. Cammi, C. Pomelli, J. W. Ochterski, R. L. Martin, K. Morokuma, V. G. Zakrzewski, G. A. Voth, P. Salvador, J. J. Dannenberg, S. Dapprich, A. D. Daniels, O. Farkas, J. B. Foresman, J. V. Ortiz, J. Cioslowski, D. J. Fox, Gaussian, Inc., Wallingford CT, **2013**.
[24] S. K. Wolff, T. Ziegler, E. van Lenthe, E. J. Baerends, *J. Chem. Phys.* **1999**, *110*, 7689.
[25] a) G. te Velde, F. M. Bickelhaupt, E. J. Baerends, C. Fonseca Guerra, S. J. A. van Gisbergen, J. G. Snijders, T. Ziegler, *J. Comput. Chem.* **2001**, *22*, 931; b) ADF2019.3, SCM, Theoretical Chemistry, Vrije Universiteit, Amsterdam, The Netherlands, https://www.scm.com; c) G. Schreckenbach, T. Ziegler, *J. Phys. Chem.* **1995**, *99*, 606–611; d) G. Schreckenbach, T. Ziegler, *Int. J. Quantum Chem.* **1997**, *61*, 899–918; e) S. K. Wolff, T. Ziegler, *J. Chem. Phys.* **1998**, *109*, 895–905.
[26] S. H. Vosko, L. Wilk, M. Nusair, *Can. J. Phys.* **1980**, *58*, 1200–1211.
[27] A. D. Becke, *Phys. Rev. A* **1988**, *38*, 3098–3100.
[28] J. P. Perdew, *Phys. Rev. B* **1986**, *33*, 8822–8824.
[29] a) M. Kállay, P. R. Nagy, D. Mester, Z. Rolik, G. Samu, J. Csontos, J. Csóka, P. B. Szabó, L. Gyevi-Nagy, B. Hégely, I. Ladjánszki, L. Szegedy, B. Ladóczki, K. Petrov, M. Farkas, P. D. Mezei, Á. Ganyecz, *J. Chem. Phys.* **2020**, *152*, 074107; b) MRCC, a quantum chemical program suite written by M. Kállay, P. R. Nagy, D. Mester, Z. Rolik, G. Samu, J. Csontos, J. Csóka, P. B. Szabó, L. Gyevi-Nagy, B. Hégely, I. Ladjánszki, L. Szegedy, B. Ladóczki, K. Petrov, M. Farkas, P. D. Mezei, Á. Ganyecz, see www.mrcc.hu.
[30] G. Schaftenaar, J. H. Nordik, *J. Comput.-Aided Mol. Des.* **2000**, *14*, 123–134.
[31] A. T. B. Gilbert, IQmol molecular viewer. Available at: http://iqmol.org (Accessed October, **2012**).

Manuscript received: October 25, 2021
Revised manuscript received: November 15, 2021
Accepted manuscript online: November 19, 2021